Supporting Information

Constructing Coordination Compound Interphases for Superior Zinc-Ion Battery Performance

Kaiyuan Zhan, Di Li, Yujuan Pu, Qiwen Zhang, Danmei Yu, Zaifang Yuan, Xiaoyu Luo, Wenjing Yang* and Xueming Li*

Experimental Section

Preparation of IA@Zn Anode: High-purity zinc foil (99.9 wt%, 100 μm thick) was ultrasonically cleaned with anhydrous ethanol and deionized water to remove surface impurities. The cleaned zinc foil was then immersed in an itaconic acid (IA) solution of a specified concentration for a set period. After immersion, the foil was rinsed three times with deionized water to remove any residual acid on the electrode surface and then vacuum-dried at 60°C for 8 hours. The resulting electrode samples are denoted as x-IA@Zn-y, where x represents the mass of IA in 60 mL of deionized water, and y indicates the immersion time of the electrode in the solution. Unless otherwise specified, x = 0.8 g and y = 10 minutes.

Preparation of MnO_2 Cathode Material: 0.25 g of carbon nanotubes were ultrasonically uniformly distributed in 1.69 g/60 mL $Mn(CH_3COO)_2{\cdot}4H_2O$ solution, and then mixed with 0.727 g/60 mL $KMnO_4$ solution and stirred continuously at 85°C for 5 hours. The resultant solid product was filtered and washed multiple times with deionized water, followed by vacuum drying at 60°C for 8 hours.

Material Characterization: X-ray diffraction (XRD) was used to obtain the crystal structure of the samples, with scans performed over a 2θ range of 5° to 90°. Scanning electron microscopy (SEM) and energy-dispersive spectroscopy (EDS) characterized the morphology and elemental distribution of the samples at an accelerating voltage of 5.0 kV. The composition of the zinc compound layer was analyzed using X-ray photoelectron spectroscopy (XPS). Contact angle measurements on the anode surface in 2 M $ZnSO_4$ solution were conducted using an XG-GAM contact angle meter at room temperature in air.

Electrochemical Characterization: Electrochemical performance tests were conducted on CR2032 coin cells using a NEWARE battery tester and CHI660E electrochemical workstation. The cells used Whatman GF/D 685 μm glass fiber membranes as separators and 2 M $ZnSO_4$ aqueous solution (100 μL) as the electrolyte. For symmetric cells, either bare Zn or IA@Zn was used as both the anode and cathode. Chronoamperometry (CA) tests were performed at a voltage of -150 mV, and electrochemical impedance spectroscopy (EIS) tests were conducted over a frequency range of 0.01 Hz to 100 kHz. Tafel curves were obtained with a voltage scan range of -0.2 V to 0.2 V and a scan rate of 1 mV s^{-1}. EIS tests for symmetric cells were also performed at temperatures ranging from 30°C to 60°C, and activation energies (Ea) were calculated using the Arrhenius equation **(eq. S1)**.

$$1/R_{ct} = A\exp\left(-E_a/RT\right) \quad \text{(S1)}$$

To calculate the transference number of zinc ions, CA tests were conducted for 1000 seconds, followed by EIS before and after the tests. The transference number was calculated using equation **(eq. S2)**, where I_0 and R_0 represent the initial current and resistance values, and I_s and R_s represent the steady-state current and resistance values, respectively.

$$t_{Zn^{2+}} = [I_s(\Delta v - I_0R_0)]/I_0(\Delta v - I_sR_s)] \quad \text{(S2)}$$

To test the coulombic efficiency, bare Zn||Cu or IA@Zn-10||Cu half-cells were assembled using a Cu foil as the cathode, bare Zn or IA@Zn-10 as the anode, and 2 M $ZnSO_4$ aqueous solution as the electrolyte. Linear sweep voltammetry (LSV) curves were tested using IA@Zn-10 or bare Zn foil as the working electrode, Ag/AgCl as the reference electrode, and a platinum wire as the counter electrode in 1 M Na_2SO_4 electrolyte. The scanning voltage range was from -1 V to -2.4 V at a scan rate of 5 mV s^{-1}.

For the full cell, a slurry consisting of MnO_2, carbon black (C), and polyvinylidene fluoride (PVDF) in an 8:1:1 ratio was prepared with N-methyl pyrrolidone (NMP) solvent using ball milling for 8 hours. The slurry was coated onto a stainless-steel foil and vacuum-dried at 80°C for 12 hours. The MnO_2 mass loading was approximately 1.5 to 2 mg cm^{-2}. The electrolyte for full cell testing was a mixed aqueous solution of 1 M $ZnSO_4$ and 0.1 M $MnSO_4$. The cyclic voltammetry (CV) curves of the full cell were scanned at a rate of 0.1 mV s^{-1}.

Computational Methods: All spin-polarised density functional theory was carried out utilizing the Vienna Ab-initio Simulation Package (VASP) to explore the structural and energetic properties of the system. The Projector Augmented-Wave (PAW) method was employed to describe the interactions between ions and electrons, and the electron exchange-correlations are described using the Perdew-Burke-Ernzerhof (PBE) functional in the generalised gradient approximation (GGA). The DFT-D3 method was also used to correct for van der Waals interactions in the structure. The plane-wave truncation energy is set to 400 eV, and the force and energy convergence criteria are 0.02 eV $Å^{-1}$ and 10^{-4} eV, respectively. The system was modeled using a 5×5 supercell to ensure sufficient sampling of the reciprocal space. A vacuum layer of 18 Å along the z-direction was employed in order to eliminate interactions between the periodic images. For k-point sampling, a Monkhorst-

Pack grid of 3×3×1 was used during geometry optimizations, while a denser 6×6×1 grid was applied in self-consistent field calculations.

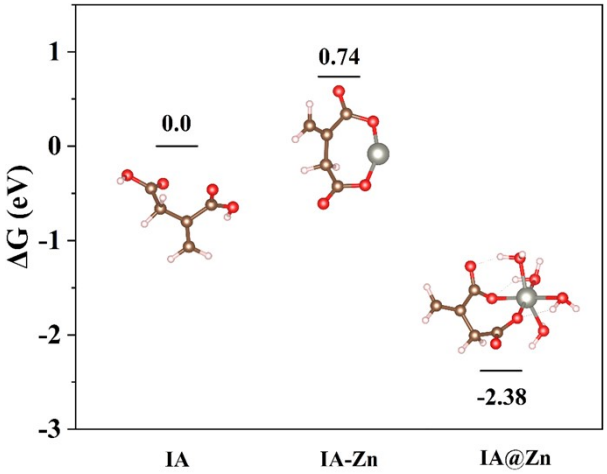

Figure S1 Gibbs Free Energy profile for the different formation of IA Complexes.

The Gibbs Free Energy calculations revealed critical insights into the stability of different structures. The formation of the IA-Zn complex from pure IA requires energy, as indicated by a positive Gibbs Free Energy Change (ΔG) of 0.74 eV. This suggests that the process is endothermic and not spontaneously favorable under standard conditions. In contrast, the formation of the hydrated complex IA@Zn (IA-Zn_4H_2O) from IA is exothermic, with a ΔG of -2.38 eV, indicating that this process releases energy and is more thermodynamically favorable. These findings underscore that in an aqueous environment, IA is more inclined to form the IA@Zn complex, which is energetically more stable.

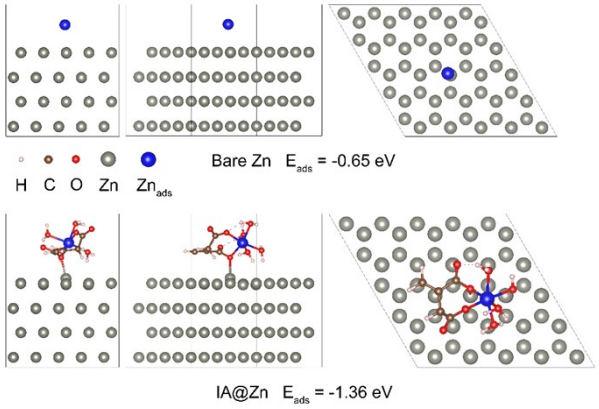

Figure S2 DFT Calculations of Zinc Atom Adsorption Energy on Bare Zn (Top) and IA@Zn (Bottom).

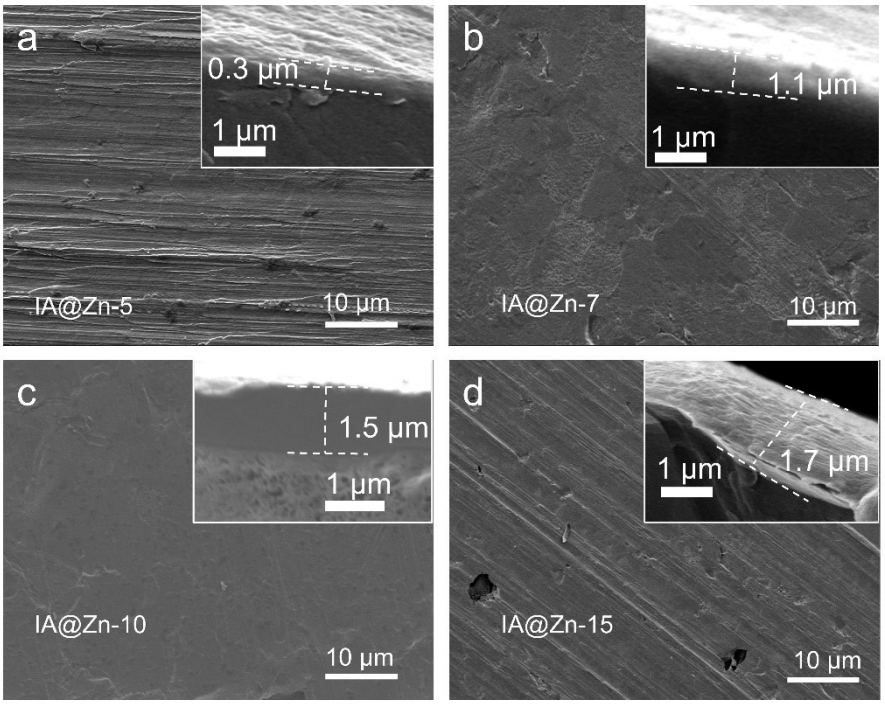

Figure S3 SEM images of the IA@Zn-y: (a) IA@Zn-5, (b) IA@Zn-7, (c) IA@Zn-10, and (d) IA@Zn-15.

The morphology of zinc foil immersed in IA solution for different durations was studied. It was found that in **Figure S3** IA@Zn-10 had the most uniform and smooth surface, while IA@Zn-15 became uneven and rough, with the appearance of holes. This was due to prolonged immersion, which caused excessive corrosion of the zinc foil, hindering the reversible deposition and stripping of zinc.

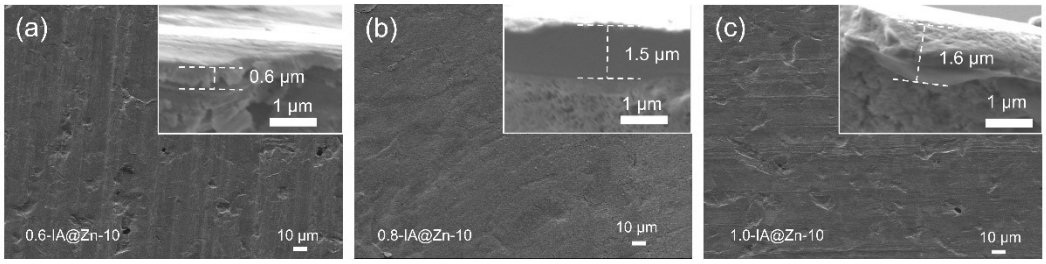

Figure S4 SEM images of the x-IA@Zn-10: (a) 0.6-IA@Zn, (b) 0.8-IA@Zn, and (c) 1.0-IA@Zn.

As shown in **Figure S4**, the 0.8-IA@Zn anode exhibits the smoothest surface, with the corresponding cross-sectional view revealing the most uniform thickness and the flattest cross-section.

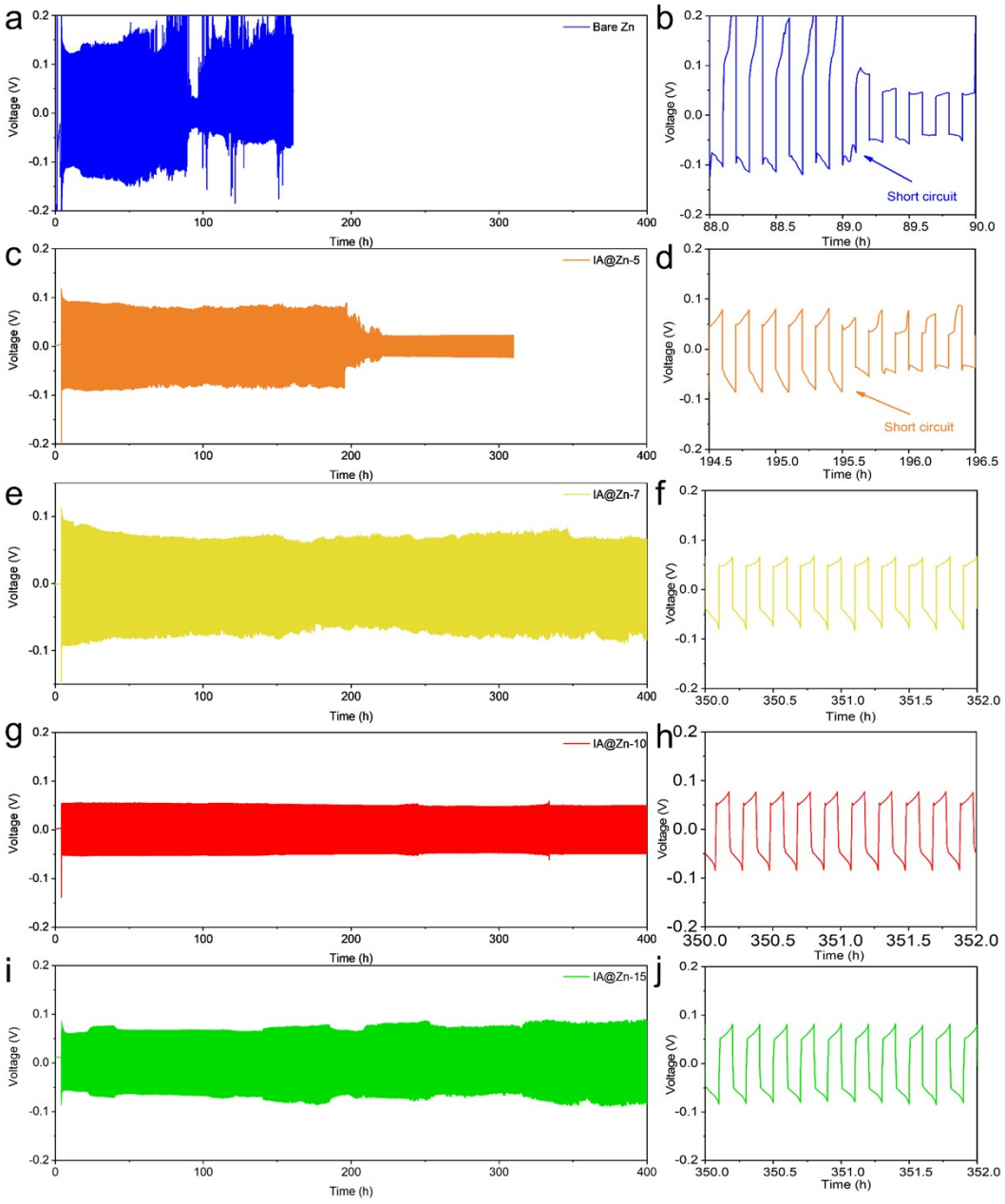

Figure S5 Long-term galvanostatic cycling and selected voltage-time profiles of (a, b) bare Zn||bare Zn, (c, d) IA@Zn-5||IA@Zn-5, (e, f) IA@Zn-7||IA@Zn-7, (g, h) IA@Zn-10||IA@Zn-10, (i, j) IA@Zn-15||IA@Zn-15 symmetric cells at 10 mA cm^{-2} with a capacity of 1 mAh cm^{-2}.

The electrochemical performance of zinc foil immersed in IA solution for different durations was also investigated. As shown in **Figure S5**, symmetric cells with bare zinc anodes exhibited a short cycle life of only 89 hours under a current density of 10 mA cm^{-2} and a capacity of 1 mAh cm^{-2}, with unstable voltage. In contrast, the cycle life of zinc anodes improved significantly after IA treatment. Specifically, while IA@Zn-5 extended the cycle life to 196 hours, IA@Zn-7, IA@Zn-10, and IA@Zn-15 symmetric cells all demonstrated cycle lives exceeding 400 hours. Notably, the IA@Zn-10 symmetric cell exhibited exceptionally high stability and ultra-low overvoltage.

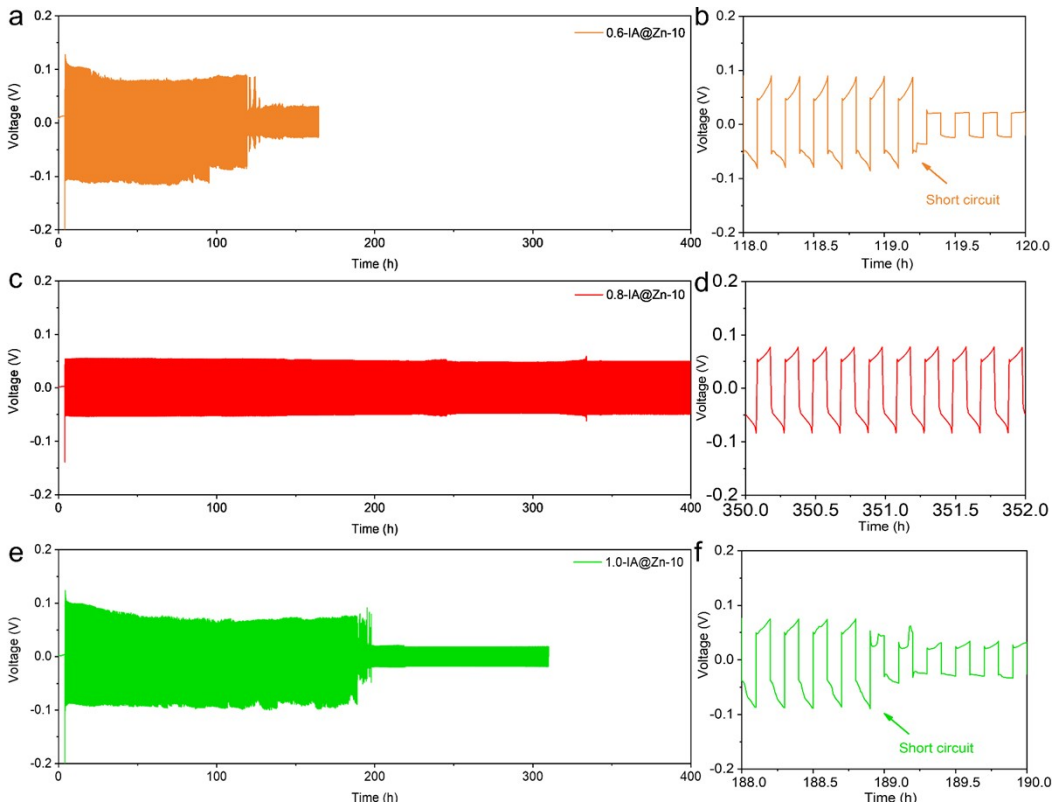

Figure S6 Long-term galvanostatic cycling and selected voltage-time profiles of (a,b) 0.6-IA@Zn-10||0.6-IA@Zn-10, (c,d) 0.8-IA@Zn-10||0.8-IA@Zn-10, (e,f) 1.0-IA@Zn-10||1.0-IA@Zn-10, symmetric cells at 10 mA cm^{-2} with a capacity of 1 mAh cm^{-2}.

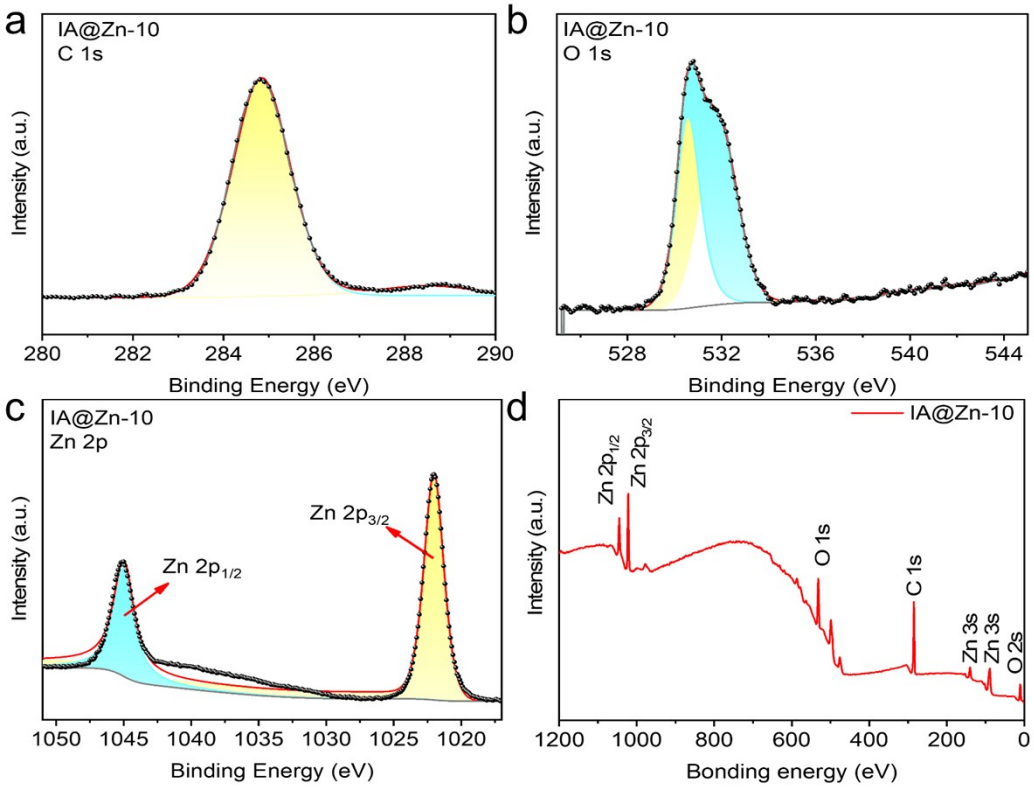

Figure S7 High-resolution XPS spectra of IA@Zn-10. (a) C 1s spectra, (b) O 1s spectra, (c) Zn 2p spectra and (d) survey spectra.

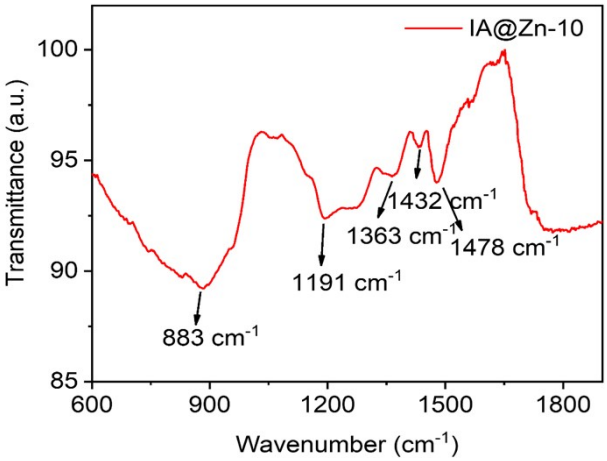

Figure S8 FTIR spectrum of IA@Zn.

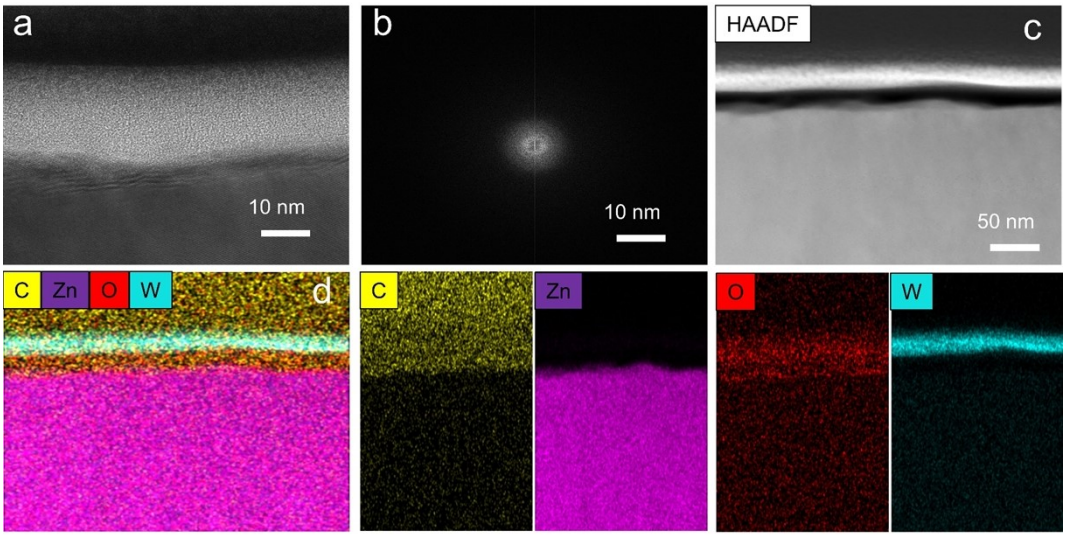

Figure S9 (a,b) High-resolution TEM images of IA@Zn. (c,d) TEM image and corresponding EDS mapping of C, Zn, O, W.

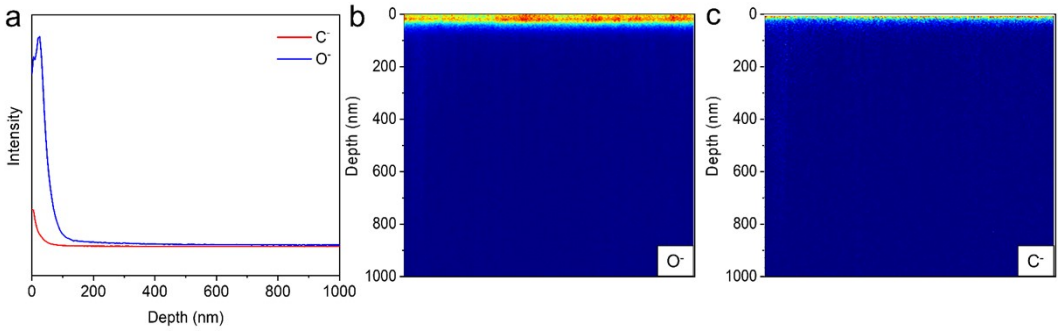

Figure S10 Anion ToF-SIMS images: (a) Depth profile of anions. (b) O^- rendered image. (c) C^- rendered image.

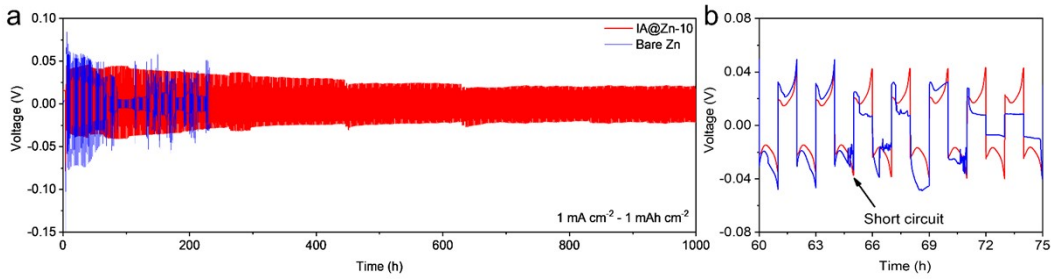

Figure S11 Long-term galvanostatic cycling and selected voltage-time profiles of IA@Zn-10 and bare Zn symmetric cells at 1 mA cm^{-2}, 1 mAh cm^{-2}.

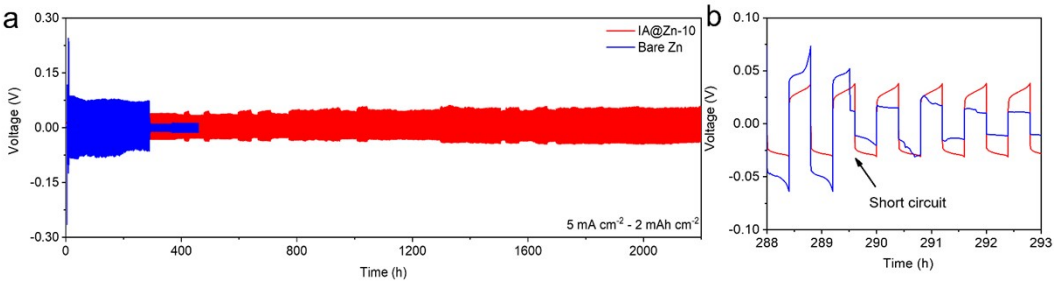

Figure S12 Long-term galvanostatic cycling and selected voltage-time profiles of IA@Zn-10 and bare Zn symmetric cells at 5 mA cm^{-2}, 2 mAh cm^{-2}.

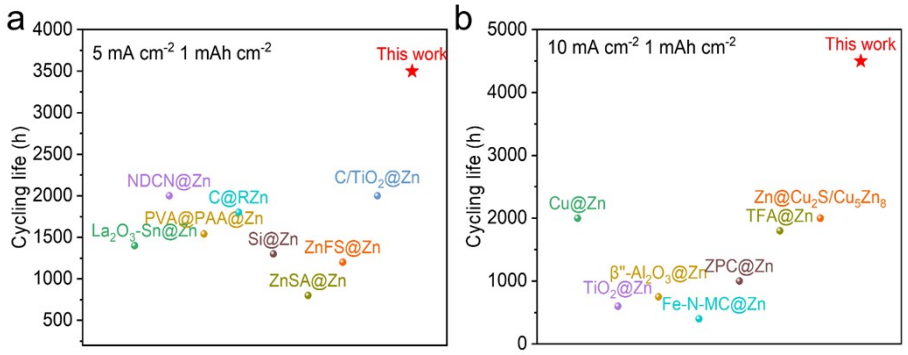

Figure S13 Comparison of the cycling life at different current densities between this work and those reported in the last two years.

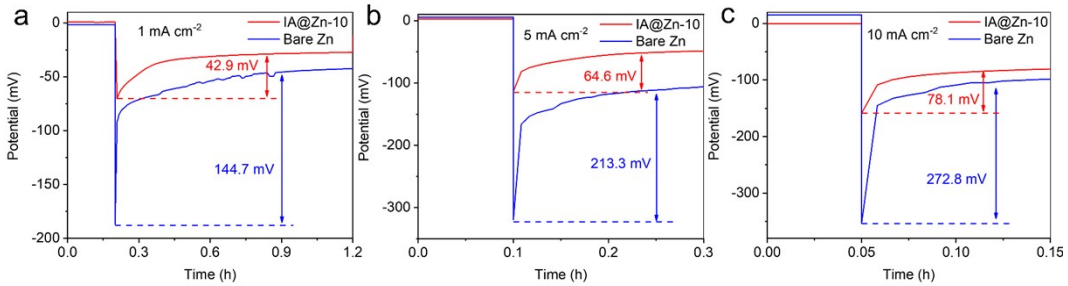

Figure S14 Nucleation overpotential of IA@Zn-10 and bare Zn symmetric cells at (a) 1 mA cm^{-2}, (b) 5 mA cm^{-2} and (c) 10 mA cm^{-2}.

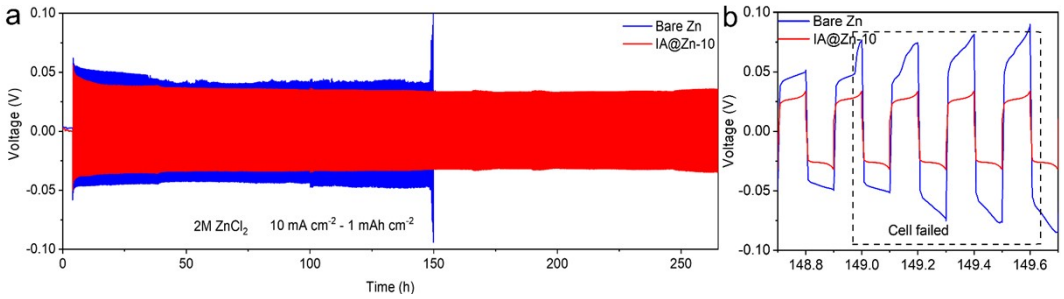

Figure S15 Long-term galvanostatic cycling and selected voltage-time profiles of symmetrical Zn||Zn cells using IA@Zn-10 and bare Zn anodes in 2 M $ZnCl_2$ at 10 mA cm^{-2}, 1 mAh cm^{-2}.

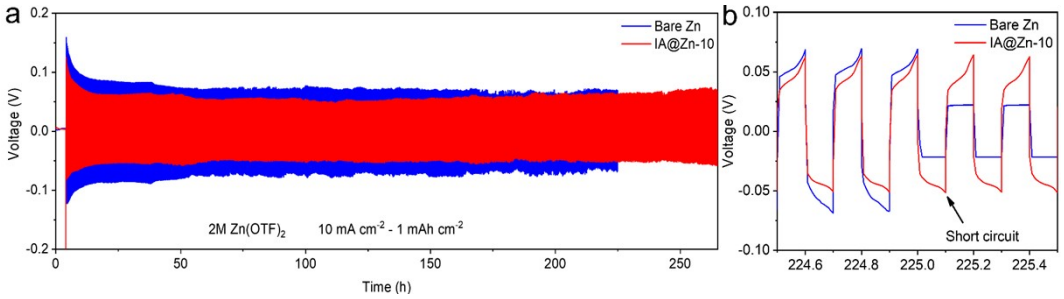

Figure S16 Long-term galvanostatic cycling and selected voltage-time profiles of symmetrical Zn||Zn cells using IA@Zn-10 and bare Zn anodes in 2 M $Zn(OTF)_2$ at 10 mA cm^{-2}, 1 mAh cm^{-2}.

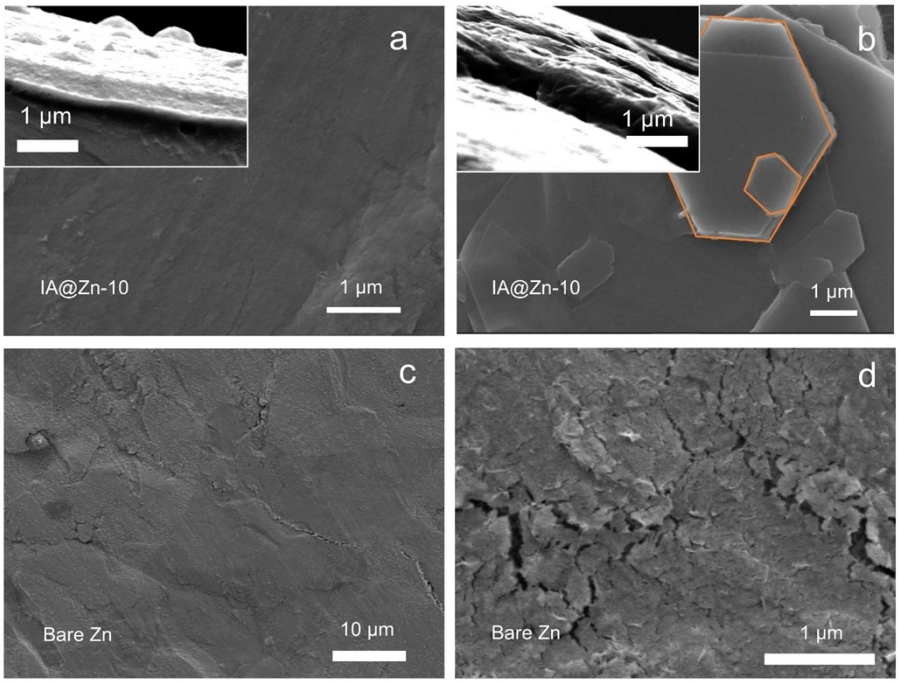

Figure S17 SEM images of cycling at 1 mA cm^{-2} and 1 mAh cm^{-2}: (a) IA@Zn-10 anode after 10 cycles, (b) IA@Zn-10 anode after 600 cycles, (c, d) bare Zn anodes after cycling for 10 cycles.

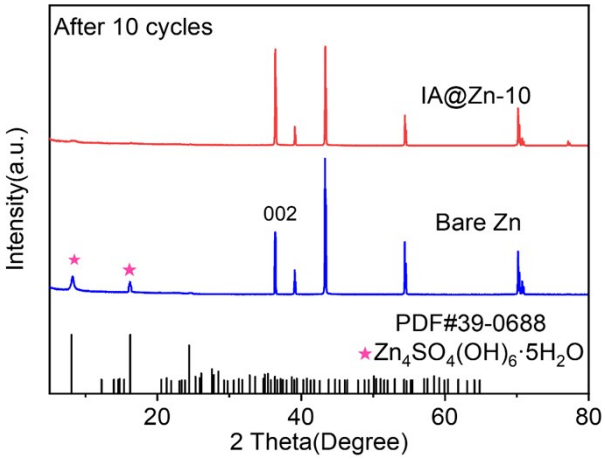

Figure S18 XRD pattern of IA@Zn-10 and bare Zn anodes after cycling for 10 cycles under 1 mA cm^{-2}, 1 mAh cm^{-2}.

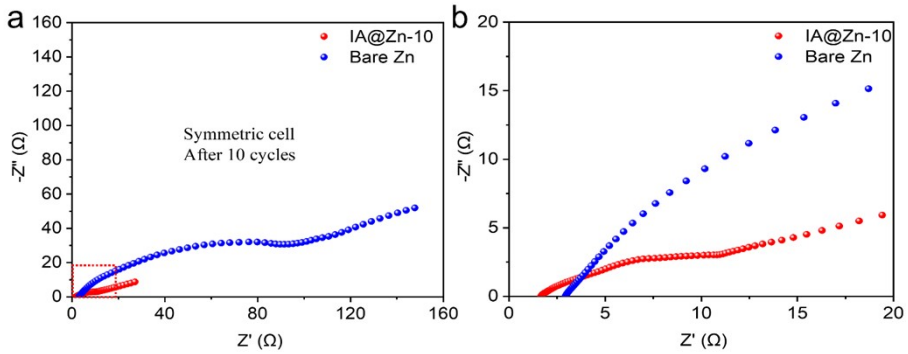

Figure S19 EIS curves of IA@Zn-10 and bare Zn symmetric cells after cycling for 10 cycles.

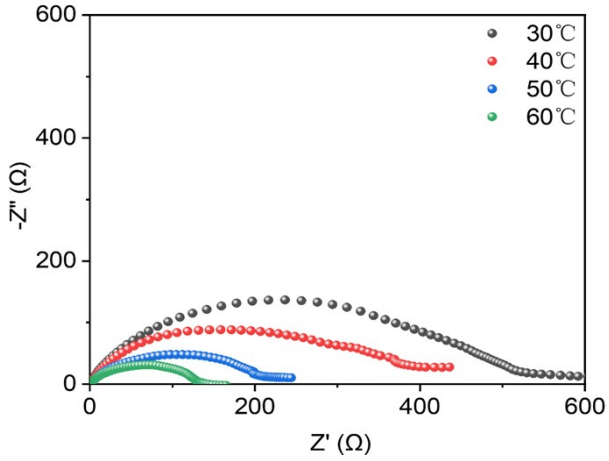

Figure S20 Nyquist plots of bare Zn||bare Zn cells at different temperatures.

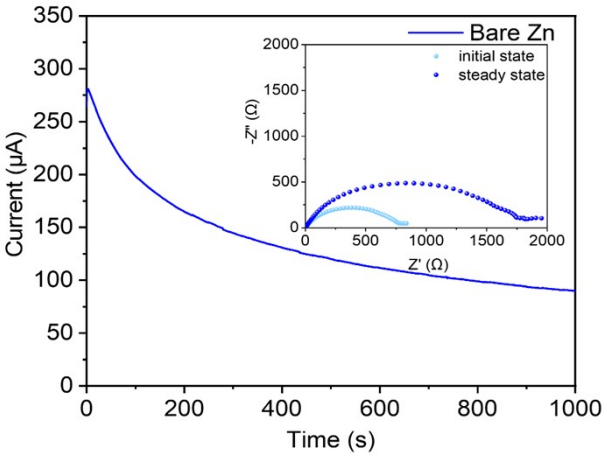

Figure S21 CA curves and the associated EIS curves of IA@Zn-10 symmetrical cells with 10 mV.

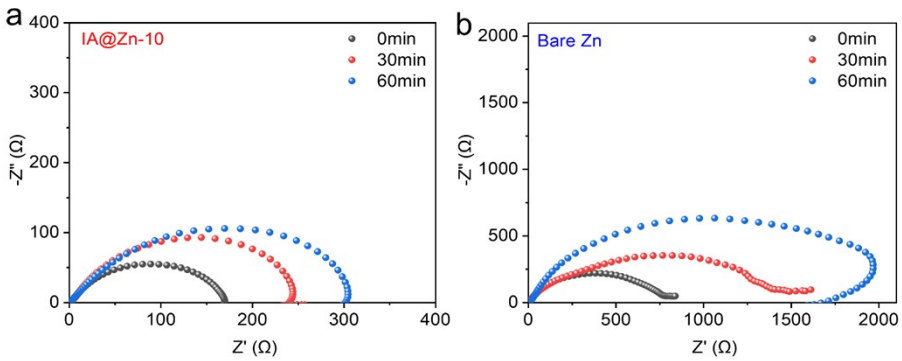

Figure S22 Time-varying impedance of symmetric cells: (a) IA@Zn-10, (b) bare Zn.

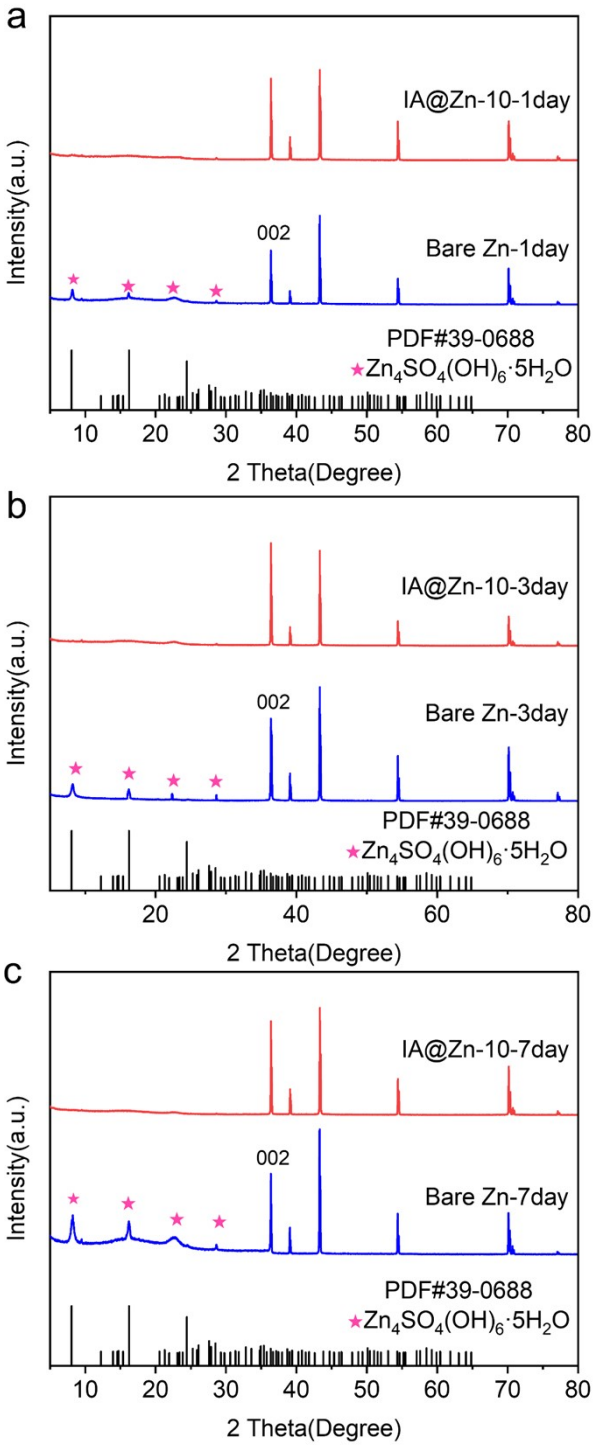

Figure S23 XRD patterns of IA@Zn-10 and bare zinc anodes immersed in 2 M $ZnSO_4$ solution for (a) 1 day, (b) 3 days, and (c) 7 days.

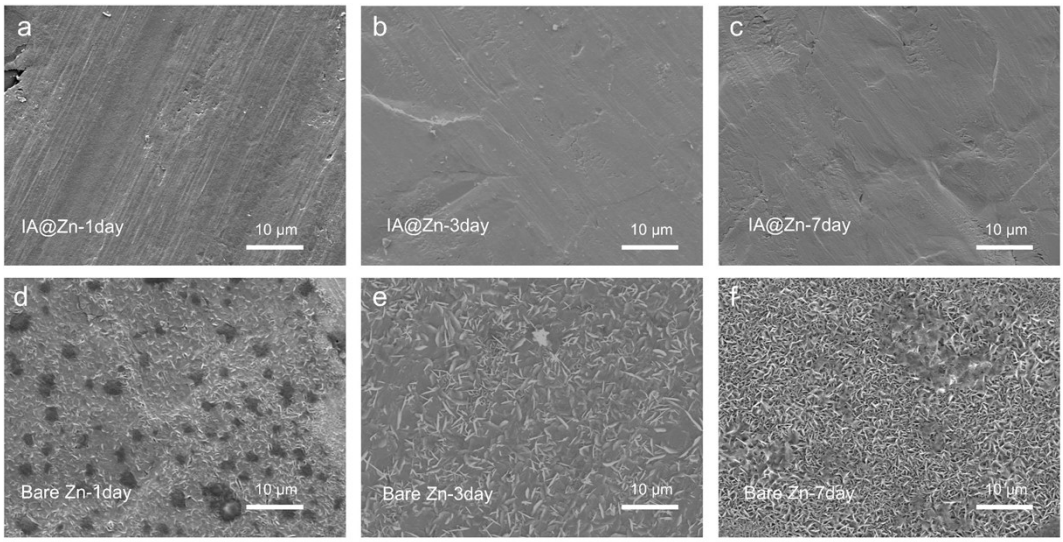

Figure S24 SEM images of IA@Zn-10 anodes after immersion in 2 M $ZnSO_4$ solution for (a) 1 day, (b) 3 days, and (c) 7 days, and bare Zn anodes for (d) 1 day, (e) 3 days, and (f) 7 days.

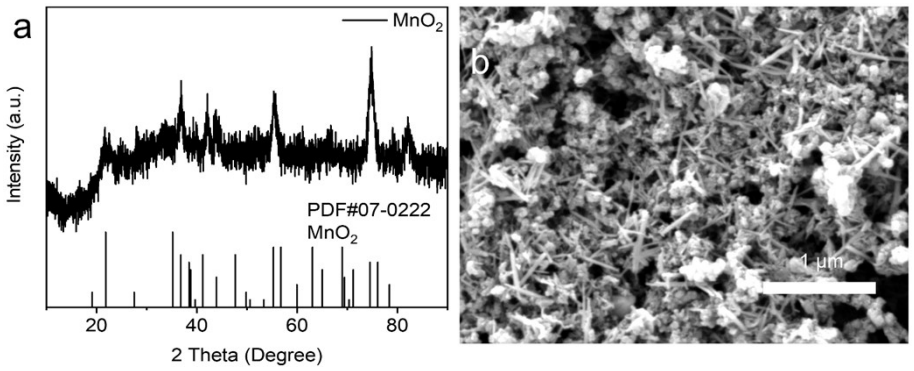

Figure S25 (a) XRD pattern and (b) SEM image of MnO_2.

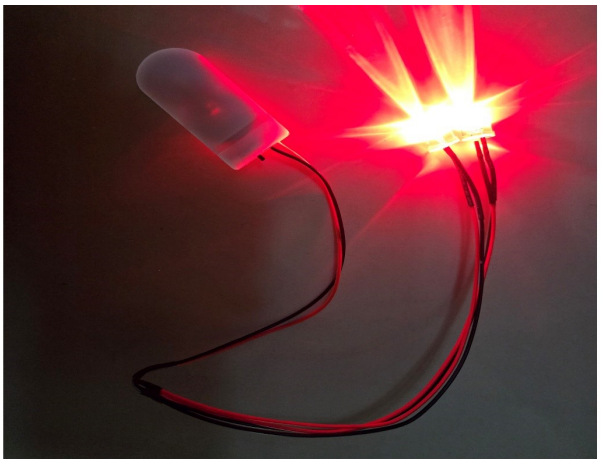

Figure S26 An image of IA@Zn-10||MnO_2 cells light up LED device.

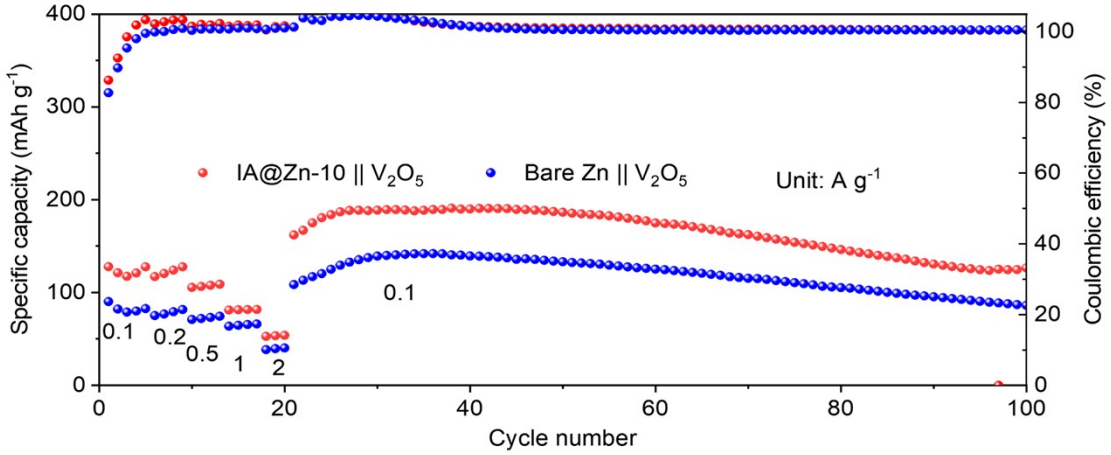

Figure S27 Cycling stabilities of IA@Zn-10||V_2O_5 and bare Zn||V_2O_5 full cells.

Table S1 Comparison of the cycling performance at a capacity of 1 mAh cm^{-2} under different current densities between this work and those reported in the last two years.

Electrode	Current density ($mA\ cm^{-2}$)	Cylcle life (h)	Ref.
This work	**5**	**3500**	
La_2O_3-Sn@Zn	5	1400	1
NDCN@Zn	5	2000	2
PVA@PAA@Zn	5	1540	3
C@RZn	5	1800	4
Si@Zn	5	1300	5
ZnSA@Zn	5	800	6
ZnFS@Zn	5	1200	7
C/TiO_2@Zn	5	2000	8
This work	**10**	**4600**	
Cu@Zn	10	1400	9
TiO_2@Zn	10	600	10
β"-Al_2O_3@Zn	10	750	11
Fe-N-MC@Zn	10	400	12
ZPC@Zn	10	1000	13
TFA@Zn	10	1800	14
Zn@Cu_2S/Cu_5Zn_8	10	2000	15

Reference

1. W. Chen, J. Tang, F. Ji, J. Sun, Q. Zhu and B.-T. Liu, *Cell Reports Physical Science*, 2023, **4**.
2. D. Zhu, J. Li, F. Ren, Y. Liu, J. Ren and Y. Xiong, *Journal of Colloid and Interface Science*, 2023, **651**, 504-513.
3. Y. Hu, H. Du, J. Lu, H. Zhang, S. Li and X. Du, *Journal of Energy Storage*, 2024, **87**.
4. M. Sun, X. Ren, L. Hu, N. Wang, Z. Gan, C. Jia and Z. Li, *Journal of Colloid and Interface Science*, 2024, **670**, 449-459.

5.Z. Dai, J. Cao, C. Yang, D. Zhang, M. Okhawilai, J. Chen, Z. Zeng, X. Zhang and J. Qin, *Journal of Alloys and Compounds*, 2023, **957**.

6.S. Lin, N. Yu, H. Wu, Y. Li, Q. Zeng, J. Li, C. Sun and K. Guo, *Applied Surface Science*, 2024, **659**.

7.Z. Hou, H. Ma, H. Tao and X.-L. Yang, *ACS Applied Materials & Interfaces*, 2023, DOI: 10.1021/acsami.3c13822.

8. Y. Zeng, H. Wang, M. Rauf, H. Mi, L. Sun, Q. Wu, Q. Zhang, X. Ren and Y. Li, *Electrochimica Acta*, 2023, **447**.
9. S.-S. Liu, Y.-R. Liang, W.-L. Chen, Z.-H. Wang, Y.-L. Dai, F.-G. Qi, Z.-S. Ma and X.-P. Ouyang, *Rare Metals*, 2024, **43**, 2125-2135.
10. W. Yang, R. Yu, S. Zhu, G. Wang, B. Zhang, J. Li, S. Xue, S. Qi, L. Zhang and K. Zhao, *ACS Applied Materials & Interfaces*, 2024, **16**, 10218-10226.
11. F. Zhang, H. Tao, Y. Li and X. Yang, *Materials Today Communications*, 2024, **39**.
12. P. Jiang, Y. Wang, Y. Li, L. Dai, N. Xu, J. Qiao and D. Ruan, *Separation and Purification Technology*, 2024, **341**.
13. X. Ye, X. Xiao, Z. Wu, X. Wu, L. Gu and S. Liu, *Journal of Energy Chemistry*, 2024, **97**, 470-477.
14. B. Kakoty and P. Senguttuvan, *Journal of Power Sources*, 2024, **594**.
15. X. He, Z. Zhu, X. Liao, K. Yang, Y. Duan, L. Lv, C. Zhao, W. Zhao, J. Chen, P. Tian, X. Liu and L. He, *Progress in Natural Science: Materials International*, 2024, **34**, 578-584.